Limnol. Oceanogr., 52(1), 2007, 184–197

Optical signatures of the filamentous cyanobacterium *Leptolyngbya boryana* during mass viral lysis

Stefan G. H. Simis,[1] *Marjolijn Tijdens, Hans L. Hoogveld, and Herman J. Gons*
Netherlands Institute of Ecology (NIOO-KNAW), Centre for Limnology, Rijksstraatweg 6, 3631 AC Nieuwersluis, The Netherlands

Abstract

The inherent optical properties of absorption and scattering, the population density of virus-like particles, and the particle size distribution (PSD) for particles >0.7 μm of the filamentous cyanobacterium *Leptolyngbya boryana* were monitored for 72 h at 9-h intervals following infection with cyanophage LPP-1. Lorenz–Mie scattering theory and the anomalous diffraction approximation were used to derive the refractive index representative of the bulk of particles and to model the particulate backscattering coefficient [$b_{bp}(\lambda)$]. Upon lysis, particulate absorption [$a_p(\lambda)$] and scattering [$b_p(\lambda)$] decreased, the number of free virus-like particles increased drastically, the PSD shifted to relative abundance of small particles, and average trichome length decreased sharply. The complex refractive index of the bulk of particles was comparable with literature values for cyanobacteria. Modeled $b_{bp}(\lambda)$ spectra were lowered upon lysis, while backscattering probability increased. The effect of underrepresentation of particles below the measurement limit of the particle sizer was studied; more small particles in the PSD resulted in higher, but still relatively low, backscattering probability. The consequences of the studied optical behavior on spectral reflectance was explored. Significant spectral changes at longer wavelengths were mostly masked by water absorption at nominal population densities. However, strongly reduced $a_p(\lambda)$ in the red pigment absorption bands resulted in a pronounced green peak in reflectance spectra, and it was concluded that reflectance band ratio algorithms targeted at the absorption of the pigments phycocyanin and chlorophyll *a* can be used to detect the mass mortality caused by viral infection. The integrated intensity of reflected light was too variable to serve as an optical indicator for lytic events.

General

Cyanobacterial blooms occur with increasing frequency in response to eutrophication of aquatic ecosystems, and they pose environmental, economic, and health threats. A potentially important role of viruses as controlling agents of phytoplankton growth has emerged from field studies on viral abundance and activity that were carried out in the last few decades (Bergh et al. 1989; Suttle 1994; Brussaard, 2004). It has become clear that viral infection can be an important mortality factor for cyanobacteria (Proctor and Fuhrman 1990; Wilson et al. 1996, 1998; Wilson and Mann 1997). In experimental conditions a seminatural cyanobacterial bloom can be lysed by viruses in the course of a few days (Van Hannen et al. 1999; Gons et al. 2002). In such experiments, changes in the inherent optical properties of particulate absorption [$a_p(\lambda)$] and scattering [$b_p(\lambda)$] were dramatic and sudden. Given the magnitude of observed optical changes, optical monitoring for catastrophic viral lysis of natural cyanobacterial populations using current remote sensing instruments seems feasible (Simis et al. 2005*b*).

Remote sensing offers the possibility of tracking optical changes in a large number of water bodies simultaneously and could thus greatly increase our understanding of the frequency and circumstances of mass lysis events. However, to evaluate mass lysis effects on remotely sensed reflectance, knowledge of the backscattering coefficient [$b_b(\lambda)$] is required, as reflectance is mainly a function of $b_b(\lambda)$ and the cumulative absorption [$a_{\mathrm{TOT}}(\lambda)$] of water [$a_w(\lambda)$] and its particulate and dissolved constituents (Gordon et al. 1975). Measurement of the particulate backscattering $b_{bp}(\lambda)$ during lysis of cultured cyanobacteria is compromised by low signal intensity, although single-wavelength scattering functions have been obtained using dedicated light scattering measurements. Balch et al. (2002) carried out such measurements on *Synechococcus* 1331 and found a decrease in $b_{bp}(514)$, but no change in the shape of the volume scattering function (VSF), upon lysis.

Upon cell lysis, a shift in the particle size distribution (PSD) from relatively large to many small particles can be observed (Shibata et al. 1997; Balch et al. 2002). In general, particles that are small with regard to the wavelength of incident light show a higher backscattering ratio [$B(\lambda) = b_{bp}(\lambda) : b_p(\lambda)$] in comparison with larger particles of the same shape and composition. The complex refractive index [$m(\lambda) = n(\lambda) + in'(\lambda)$] of the cell material and the particle size relative to the wavelength of incident light jointly define the VSF. Increased $B(514)$ was recorded for bacterial cultures, but not for cyanobacteria (Balch et al. 2002). For

[1] Corresponding author (s.simis@nioo.knaw.nl).

Acknowledgments

We thank Hans van der Woerd, Hester Volten, and two anonymous reviewers for their comments, which helped to improve the manuscript.

Funding for this work was provided through grant EO-053 from the User Support Programme, managed by the programme office of the External Research of the Netherlands Organization for Scientific Research—National Institute for Space Research (NWO-SRON). Part of the work was carried out at the Institute for Environmental Studies, Vrije Universiteit, Amsterdam.

This is publication 3937, NIOO-KNAW Netherlands Institute of Ecology, Centre for Limnology.

phototrophs, changes in $m(\lambda)$ as a result of cell lysis have not been reported.

The scenario of mass lysis of a bloom-forming species that dominates the optical properties of the water column can be approached experimentally. The present study focuses on the optical changes of the cultured filamentous cyanobacterium *Leptolyngbya boryana* infected with cyanophage LPP-1. Measurements of $a_p(\lambda)$, $b_p(\lambda)$, and the PSD were carried out at regular intervals until the infected cultures had visibly cleared. Subsequently, $b_{bp}(\lambda)$ was obtained from the best fit of the measured and modeled optical properties through a Mie–Lorenz scattering model for homogeneous spherical particles, which uses $m(\lambda)$ and relative particle size as input. The approach was first described by Morel and Bricaud (1986) and was adapted as described below.

Scattering model

Lorenz–Mie theory and its later formulations, commonly referred to as Mie theory (Mie 1908), can be used to describe light propagation by simultaneously scattering and absorbing spherical particles, through electromagnetic wave theory. For a single spherical particle with known diameter and $m(\lambda)$, the model yields the efficiency of light absorption and angular scattering. For a polydisperse population of irregularly shaped particles in random orientation, the assumption that particles are perfect spheres may be relaxed (Latimer et al. 1978; Bohren and Huffmann 1983; Morel and Bricaud 1986). This generalization has been repeatedly put to use in hydrologic optics to explain the scattering contributions of the various biological elements of aquatic ecosystems (Morel and Ahn 1991; Stramski and Kiefer 1991; Stramski and Mobley 1997). The approximation of Mie scattering made using anomalous diffraction theory (ADT) may be used as an alternative to derive $m(\lambda)$ (Van de Hulst 1957). It is not possible to calculate the angular distribution of propagated light with ADT, so its use is restricted to fitting $m(\lambda)$ to the optical and PSD measurements. Combining Mie theory and ADT, Morel and Bricaud (1986) modeled the light propagation by picoplanktonic cyanobacteria. Ahn et al. (1992) extended the modeling approach to cultured phytoplankton species of various shapes, sizes, and plankton subgroups. In Volten et al. (1998), a wide range of phytoplankton groups and some silt samples were described both with Mie scattering calculations and VSF measurements at wavelength (λ) = 633 nm. The latter study pointed out some of the difficulties with fitting the Mie model to optical measurements. This was particularly apparent for filamentous and other colony-forming species, in which some values of $m(\lambda)$ fitted by the model were implausibly high. The present study also used the Mie approach to model scattering by filamentous cyanobacteria. However, instead of using volume-equivalent spheres to represent whole trichomes, as was the case in the earlier work, we entered spheres into the model to represent individual cells, regardless of their position in a colony structure. This approach may result in more realistic values of $m(\lambda)$.

Mass lysis of host cells is expected to cause a shift in the PSD toward smaller particles as cell walls are disrupted and cell debris is released at the final stage of infection. With smaller particle size, relative to the wavelength of incident light, the scattered light field becomes more diffuse. In many natural situations, submicron-sized particles (SMP) and colloids contribute significantly to the total backscattering (Morel and Ahn 1991; Stramski and Kiefer 1991; Ulloa et al. 1994; Stramski and Wozniak 2005). The role of SMP with regard to $b_{bp}(\lambda)$ has not been studied during dense cyanobacterial bloom but may become important as a result of sudden mass lysis. Previously, the number of particles released per lysed cell was estimated to be around 20 for bacterial cells (Shibata et al. 1997). In the present study, the effect of SMP on modeled $b_{bp}(\lambda)$ and $B(\lambda)$ is investigated, prompted by the fact that the used particle sizer was insensitive to SMP of <0.7 μm. Considering cases during mass lysis with limited and exaggerated numbers of expected SMP, it is possible to explore the sensitivity of modeled $b_{bp}(\lambda)$ and $B(\lambda)$ to the changes in the PSD.

Finally, using both measured $a_p(\lambda)$ and modeled $b_{bp}(\lambda)$, the effect of mass viral lysis on remotely sensed reflectance of inland and coastal waters exhibiting cyanobacterial blooms can be assessed.

Methods

Cell cultures and experimental conditions—The cyanobacterial host *Leptolyngbya boryana* (Gomont) Anagnostidis et Komárek (1988), previously *Plectonema boryanum*, and the cyanophage LPP-1 were obtained from the American Type Culture Collection. The host was grown on modified Chu 10 medium, and LPP-1 stock was regularly harvested from infected cultures and stored in a magnesium salt solution (Safferman and Morris 1964). A week before and then again several days before the start of the experiment the host was transferred to fresh culture medium and kept at the same temperature and ambient light used during the experiment. The culture flasks were placed on an orbital shaker in an incubator and supplied with continuous light (Sylvania Britegro fluorescent tubes) at approximately 95 μmol quanta m^{-2} s^{-1} photosynthetically active radiation. Temperature was maintained at 20°C. Several hours before the start of the experiment, 50 mL of the culture stock and 50 mL of fresh culture medium were added to four 250-mL Erlenmeyer flasks. At t = 0, three flasks received 0.750 mL of LPP-1 phage stock (adding approximately 1×10^8 viruses mL^{-1} $flask^{-1}$). As a negative control treatment a fourth flask received 0.750 mL phage-free magnesium salt solution. Low densities of heterotrophic bacteria were maintained in the host cultures, growing on dying *L. boryana* cells and exudates; the culture medium alone did not support growth of these bacteria. They were included in the experiment to cause degradation of the lytic material, above all the water-soluble phycobilin pigments that can be released from lysing cells. The heterotrophic bacteria were rod-shaped, with a narrow size distribution around a volume-equivalent sphere diameter (ESD) of 0.95 ($\pm$0.11) μm. The cultures were treated under sterile conditions, and we periodically

Table 1. List of recurrent symbols.

Symbol	Description	Units
λ	Wavelength of light in air	μm or nm
a	Absorption coefficient	
a_p	Particulate absorption coefficient, assuming negligible absorption by dissolved matter	m^{-1}
a_w	Absorption coefficient of pure water	m^{-1}
a_{TOT}	$a_w + a_p + a_{CDOM}$	m^{-1}
b	Scattering coefficient	
b_p	Particulate scattering coefficient	m^{-1}
b_b	Backscattering coefficient	m^{-1}
b_{bp}	Particulate backscattering coefficient	m^{-1}
c	Beam attenuation coefficient	m^{-1}
c_p	Particulate beam attenuation coefficient	
B	Backscattering probability, ratio $b_{bp}:b_p$	Dimensionless
$R(0^-)$	Subsurface irradiance reflectance at depth 0	Dimensionless
ω_b	Backscattering albedo, $b_{bp}(\lambda)/[a_{TOT}(\lambda) + b_{bp}(\lambda)]$	Dimensionless
m	Complex refractive index relative to water	Dimensionless
n	Real part of m	Dimensionless
n'	Imaginary part of m	Dimensionless
Q_j	Optical efficiency factor of a particle ($j = a$, b, c, or b_b)	Dimensionless
$\bar{Q}_j$	Optical efficiency factor of the 'average' particle ($j = a$, b, c, or b_b)	Dimensionless
d	Particle diameter	μm or m (Eq. 1)
x	Particle size relative to wavelength of light in surrounding medium	Dimensionless
S	Geometric shape factor of bulk of particles	m^{-1}
$S(d)$	Geometric shape factor of particle with diameter d	m^{-1}

checked to ensure that no phototrophic species other than *L. boryana* were present.

Virus-like particles—Free virus-like particles (VLP) were enumerated according to Noble and Fuhrman (1998). In short, diluted samples were filtered over 0.02-μm pore size, 25-mm–diameter Anodisc (Whatman) filters and stained with SYBR Green I (Molecular Probes). At least 200 VLP were counted using a Zeiss Axiophot epifluorescence microscope using blue light for excitation.

Measured inherent optical properties—Measurements of the inherent optical properties were made with a Lambda 800 UV/Vis spectrophotometer (PerkinElmer) in the 350–800-nm wavelength (denoted λ; refer to Table 1 for a list of recurring symbols) range. Absorbance spectra were measured by placing a 1-cm–path length quartz cell, with clear panes on all sides, in the center of a 150-mm integrating sphere accessory (Labsphere). The measured absorbance spectra were obtained from the spectral difference between the sample and the cuvette filled with 0.2-μm filtered distilled water. The spectra were scaled to absorption units to yield $a(\lambda)$. Various papers discuss the method of measuring absorption inside an integrating sphere in detail (Maske and Haardt 1987; Babin and Stramski 2002, 2004).

The beam attenuation coefficient [$c(\lambda)$] was measured in a 1-cm–path length cuvette against a reference of filtered distilled water. The spectrophotometer was set up in dual-beam mode for this measurement, the cuvette positioned at a relatively large distance from the detector (0.20–0.25 m) to exclude detection of light scattered at angles above an estimated 1.3°. Details on the spectrophotometric determination of $c(\lambda)$ and dependence on detector acceptance angle may be found elsewhere (Bricaud et al. 1983; Stramski and Reynolds 1993). Spectra of $b(\lambda)$ were obtained from the difference between $c(\lambda)$ and $a(\lambda)$.

To minimize the possibility of multiple scattering during measurement of $a(\lambda)$ and $c(\lambda)$, dilutions of the sample were made until the optical thickness [the product of $c(\lambda)$ and path length] was below 0.3 (Bricaud et al. 1988). All spectrophotometric measurements were made at 1-nm intervals, with an integration time of 0.24 s nm^{-1} and a slit width of 2 nm. A correction of $a(\lambda)$, made by subtracting near-infrared values, was not needed, as scattering losses were negligible when the sample was placed in the center of the sphere.

The absorption by colored dissolved organic matter (CDOM) was obtained from the filtrate of samples passed over a 0.2-μm Schleicher & Schuell FP30 cellulose acetate membrane filter that was pre-rinsed with the sample. These measurements were carried out as described for measurement of $a(\lambda)$, inside the integrating sphere. CDOM contribution to the absorption measured from suspensions was low (<5% in the measured wavelength range) throughout the experiment. Because the influence of the dissolved fraction on the total absorption was low, the beam attenuation, absorption, and scattering measurements described above were adopted for the particulate beam attenuation [$c_p(\lambda)$], particulate absorption [$a_p(\lambda)$], and particulate scattering [$b_p(\lambda)$].

Particle size distribution—The PSD was obtained from microscopic observations combined with size distribution measurements using a Casy TTC particle sizer (Schärfe System GmbH). This particle sizer detects particle volumes by integrating changes in an electromagnetic field at a frequency of 1 MHz as particles pass through a capillary. Lower and upper detection limits were 0.18 μm^3 (0.7 μm

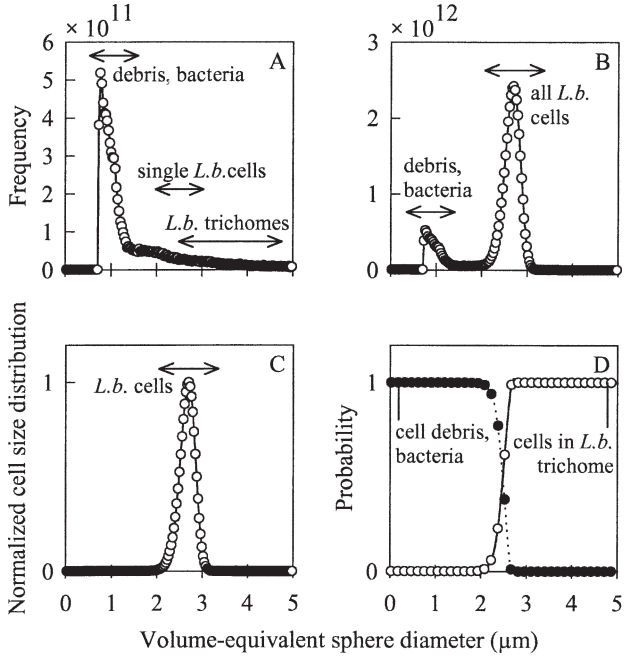

Fig. 1. Procedure followed to obtain the particle size distribution (PSD) from microscopic observations of cell size and from automated particle counts that include *L. boryana* trichomes. The displayed results are expressed in volume-equivalent sphere diameter at the size classes used as input for the scattering model, for the average of infected cultures at $t = 0$. (A) Particle sizer output showing peaked distribution toward smaller diameters. Heterotrophic bacteria constitute part of the peak, with an ESD of approximately 1 μm. (B) Final PSD, combining particle sizer output and microscopically observed cell size distribution. The sum of single *L. boryana* cells and cells organized in trichomes yields the peak at 2–3 μm; the peak that constitutes smaller particles is the same as in panel A (note difference in scale). (C) Normalized size distribution of *L. boryana* cells, based on Gaussian fit of microscopic observations of cells organized in trichomes of greater than or equal to one cell length. (D) Probability functions used to distinguish *L. boryana* cells (either single or organized in trichomes) from smaller particles like cell debris and heterotrophic bacteria.

ESD) and 14,137 μm^3 (30 μm ESD), which amply covers the range of expected volumes of *L. boryana* trichomes as well as most of the heterotrophic bacteria present.

The particle sizer initially detected cyanobacterial trichomes as single particles that have a relatively large ESD. However, individual cells conform better to the assumption of sphericity by the Mie model than do trichomes. The PSD obtained by the particle sizer (*see Fig. 1A* for $t = 0$ h) was therefore converted so that the PSD ultimately used as model input (Fig. 1B) included individual *L. boryana* cells as well as cell debris and heterotrophic bacteria. Microscopic examination of the samples yielded the distribution of cyanobacterial cell volumes, which was fitted by a Gaussian curve (Fig. 1C). The cell volumes and ESD were calculated from cell length and diameter assuming a cylindrical cell shape. A probability function was constructed from the fitted ESD distribution to separate the total volume measured by the particle sizer into the volumes contained in small particles (debris, bacteria) and *L. boryana* cells (Fig. 1D). Per size class, the product of total volume (particle sizer) and the probability of any *L. boryana* cells present yielded the volume contained in *L. boryana* cells. This volume then yielded the number of *L. boryana* cells, using the average cell volume obtained from microscopy. The final PSD (Fig. 1B) was then built from the sum of individual *L. boryana* cells and all smaller matter, repeated for each size class. It is noted that the samples for microscopic determination of cell dimensions were fixed with a minimal amount of Lugol's solution. The samples were kept at 4°C and were analyzed within 3 weeks after the experiment. No marked effect of the fixative on cell size was observed compared to regular observations of fresh *L. boryana* cultures. The PSD data were reduced to 44 size classes in the range of 0–7 μm ESD. Values of ESD given in the text and figures of this paper refer to the midpoint of these classes, which are plotted as symbols in Fig. 1.

Optimization of the refractive index—The optical efficiency factor of the 'average' particle, $\bar{Q}_j(\lambda)$ ($j = a$, b, c, or b_b), can be determined from the PSD and the optical coefficients $a_p(\lambda)$ and $b_p(\lambda)$. The PSD is first converted into the geometrical shape factor for the whole population (S) following

$$S = \sum_{C=1}^{n} (\pi/4) \times d_C^2 \times N_C \quad (1)$$

where C is size class number, d_C the particle diameter describing the size class, and N_C the number of particles in a size class per unit volume of medium. The unit of S is m^{-1}. By convention, the unit for particle diameter d is μm; however, exclusively in Eq. 1, d is expressed in m.

For the whole population of suspended particles,

$$\bar{Q}_j(\lambda) = j(\lambda)/S \quad (2)$$

The ADT and Mie models use the relative particle size and $m(\lambda)$ as input parameters. The relative particle size is expressed as the dimensionless size parameter x

$$x = \pi\, d\, n_w(\lambda)/\lambda \quad (3)$$

where $n_w(\lambda)$ is the refractive index of the medium (water) and λ the wavelength (in μm) of the light in air. Only the real part of $n_w(\lambda)$ is used here, as the value of the imaginary part is low over the entire 350–800-nm range, with a maximum $< 1.6 \times 10^{-7}$ around 750 nm. The real part of $n_w(\lambda)$ was interpolated from Segelstein (1981), although a fixed value of 1.33 did not yield significantly different results. The values of $m(\lambda)$ are also expressed relative to the refractive index of the medium.

ADT calculations gave the optical efficiency factors for a single size class, $Q_j(\lambda)$. To obtain $\bar{Q}_j(\lambda)$, calculations for every size class were made and weighted according to their shape factors (from Eq. 1, it follows that $S(d) = \pi/4\, d^2\, N$). Because $\bar{Q}_j(\lambda)$ could thus be derived from both measured and modeled optical properties, it was possible to optimize the value of $m(\lambda)$ for the best fit of measured and modeled

optical efficiencies. If $\Delta Q_f(\lambda)$ is the absolute difference between measured and modeled $\bar{Q}_f(\lambda)$, then the optimal value of $m(\lambda)$ leads to the smallest value of $[\Delta Q_a(\lambda) + \Delta Q_b(\lambda)]$. The optimization routine outlined below was mainly adapted from earlier publications (Morel and Bricaud 1986; Stramski et al. 1988) to quickly retrieve $m(\lambda)$ for the wavelength range 350–800 nm at 1-nm intervals. All calculations were made for the polydisperse population. First, a plausible value of $m(\lambda)$ was chosen as a starting value, and after every iteration, the optimized value was used as a starting point for the next wavelength in the series. This approach speeds up the optimization process, as differences in $m(\lambda)$ are typically small at 1-nm intervals. Convergence of modeled and measured optical efficiency factors was reached for all samples at all wavelengths when starting from 800 nm with $m = 1.02 + 0.003i$ and proceeding toward shorter wavelengths, starting with the optimized value of the last step. The optimization routine itself was structured so that a 5×5 matrix around the initial value of $m(\lambda)$ was constructed, with a variation of 10% and 20% around $m(\lambda)$ for both the imaginary part (n') and the real part above 1 ($n - 1$). If negative values of $n - 1$ or n' occurred in the matrix, these were zeroed. The value from the m-matrix that yielded the best fit of modeled and measured efficiency factors was selected, and a new matrix around this value was constructed. The procedure was then repeated until no change in the optimal value of $m(\lambda)$ was found. Variation in the m-matrix was subsequently reduced to 1% and 2% around $m(\lambda)$ until the procedure again yielded no change. The optimal value of $m(\lambda)$ was then stored, and the routine was started for the next wavelength in the series.

The optimization procedure was carried out using the ADT routine, after it was confirmed that during test runs the ADT and Mie models gave the same optimized value of the refractive index, within 1%, for selected samples at 10-nm intervals. The ADT routine does not yield angular scattering coefficients, so the Mie routine was still operated on the optimized values of $m(\lambda)$ for every sample, wavelength, and size class. The obtained efficiency factors for every size class were multiplied by the size class's respective shape factor and particle density, yielding the modeled inherent optical property $b_{bp}(\lambda)$.

The measurements of $a_p(\lambda)$, $b_p(\lambda)$, and PSD for the replicate infected samples were averaged before operating the scattering models. No smoothing of spectral data was carried out except for plotting some of the figures (as indicated).

Reflectance—For the interpretation of remotely sensed signals it has been established that the reflectance of solar irradiance at zero depth $[R(0^-, \lambda)]$ is related to the inherent optical properties of the water column through (Gordon et al. 1975, eq. 20)

$$R(0^-, \lambda) = f\{b_b(\lambda)/[a_{\mathrm{TOT}}(\lambda) + b_b(\lambda)]\} \quad (4)$$

where f is a scaling factor dependent on the incident light field (Morel and Gentili 1991, 1993). The term $a_{\mathrm{TOT}}(\lambda)$ sums the absorption by water and its constituents $[a_w(\lambda) + a_p(\lambda) + a_{\mathrm{CDOM}}(\lambda)]$. The absorption by CDOM $[a_{\mathrm{CDOM}}(\lambda)]$ did not significantly contribute to $a_{\mathrm{TOT}}(\lambda)$ and was omitted. The absorption by pure water $[a_w(\lambda)]$ was obtained from Buiteveld et al. (1994). The dimensionless bracketed term can be considered an inherent optical property of the water body, closely related to subsurface reflectance but not dependent on the incident light field. By analogy to the scattering albedo $\omega(\lambda)$, the term is defined here as the backscattering albedo, calculated as $\{\omega_b(\lambda) = b_{bp}(\lambda)/[a_{\mathrm{TOT}}(\lambda) + b_{bp}(\lambda)]\}$. Spectra of $\omega_b(\lambda)$ were calculated from modeled $b_{bp}(\lambda)$ and measured $a_p(\lambda)$.

Results

As soon as 18 h after infection, the length of trichomes in the infected cultures decreased drastically (Fig. 2A). Average trichome length of the control culture exceeded 100 cells per trichome nearing the end of the experiment, while in infected cultures the average was <5 cells per trichome from 18 h after infection onward. After 36 h, average filament length was ≤ 3 cells, and at $t = 72$ h, no intact cyanobacterial cells were observed. Both the infected cultures and the control culture exhibited an increase in average cell volume from the start of the experiment, caused by an increase in average cell length, while average diameter remained constant (Fig. 2B). The increase in length may be attributed to two processes. First, in infected cultures, trichomes split up into many smaller sections, and, thus, relatively many cells were located at the apical ends of trichomes, which are slightly elongated. Second, growth of *L. boryana* follows a regular pattern of increase in cell length and subsequent cell division. Because the culture medium was refreshed twice shortly before the start of the experiment, using a small inoculum, cell division could have been synchronized. Although the two processes affected the treatments differently, no significant difference in the trend of cell length and volume was found between control and infected cultures.

Temporal changes in PSD differed markedly between the control and infected cultures. The PSD for both treatments was plotted in Fig. 3, where a band around ESD = 3 μm represents the *L. boryana* cells, and the band around ESD = 1 μm represents heterotrophic bacteria and cell debris. Some variation in peak height was observed in the control treatment for the smaller particles, close to the detection limit of the particle counter at ESD = 0.7 μm. This variation is attributed to instrument noise—it was also present between repeated counts of individual samples. The infected cultures consisted of three replicate samples instead of one for the control treatment, which canceled out most instrument noise. The increase of average cell length and volume with time, as discussed above, was reflected in the PSDs, as the band around ESD = 3 μm shows a shift to larger ESD for both infected and control cultures.

Optical measurements showed differences between control and infected treatments from $t = 9$ h. Absorption by CDOM increased slightly upon lysis but remained low (results not shown). The lack of CDOM increase may be

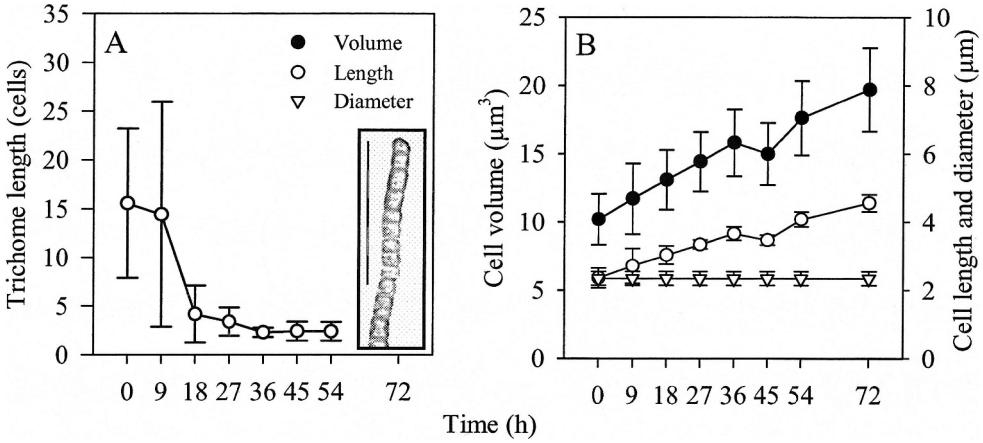

Fig. 2. Microscopic observations of (A) average and standard deviation of trichome length, for infected cultures, and (B) average and standard deviation of cell volumes, cell length, and cell diameter for a combination of infected ($n = 3$) and control ($n = 1$) cultures. Cell morphology did not differ between infected and control cultures. The data at $t = 72$ h is based only on the cells in the control culture, as no cells were found in the infected cultures. The inset in panel A shows a light microscope image of a fragment of a *L. boryana* trichome; the scale bar measures 20 μm.

attributed to the presence of the heterotrophic bacteria, which are also considered to be responsible for a lack of water-soluble pigments visible in the dissolved fraction. Only around $t = 18$ h was weak absorption observed around the absorption peaks of the pigments phycocyanin (PC, around 615 nm) and chlorophyll *a* (Chl *a*, around 440 nm and 675 nm), close to the detection limit of the spectrophotometer. It was previously described that Chl *a*–like absorption patterns in the CDOM fraction (<0.2 μm) during mass lysis of cyanobacteria have a particulate nature (Simis et al. 2005*b*). The absence of significant absorption in this experiment thus indicates that the degradation of lytic matter either took place very rapidly or that the cell fragments released during this experiment were mostly larger than 0.2 μm. We tested whether the scattering models gave different results when the weak CDOM absorption was included in the imaginary part of n_w, which was not the case. Therefore, CDOM absorption was further neglected.

Measured $a_p(\lambda)$ and $b_p(\lambda)$ continuously increased in the control culture (Fig. 4A,C). A marked increase in the blue to green domain was observed, whereas the increase in the red part of the spectrum was small. This indicated that the culture was light saturated and produced more photoprotective carotenoid pigments than photosynthetic pigments. In contrast, the infected cultures showed a drastic decline in both $a_p(\lambda)$ and $b_p(\lambda)$ (Fig. 4B,D). The first change appeared to be loss of PC, which showed at $t = 9$ h as decreasing absorption around 620 nm, while the rest of the spectrum appeared unaffected. From $t = 9$ h toward the end of the experiment, an overall decrease and flattening of $a_p(\lambda)$ was observed. The infected cultures showed an initial

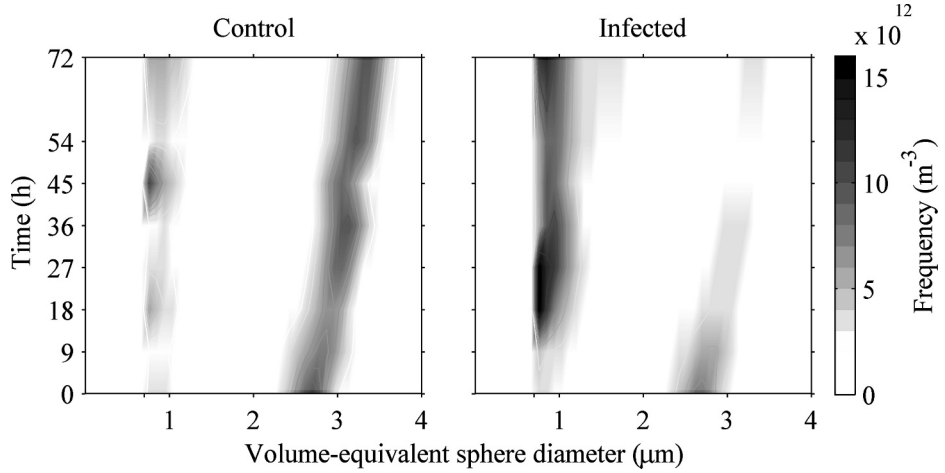

Fig. 3. Particle size distributions after conversion of trichomes to individual cells (*see Methods and Fig. 1*). Cells are visible as a band around ESD = 3 μm; cell fragments and heterotrophic bacteria are visible around 1 μm. Frequencies (gray scale) were linearly interpolated between sampling times and size classes.

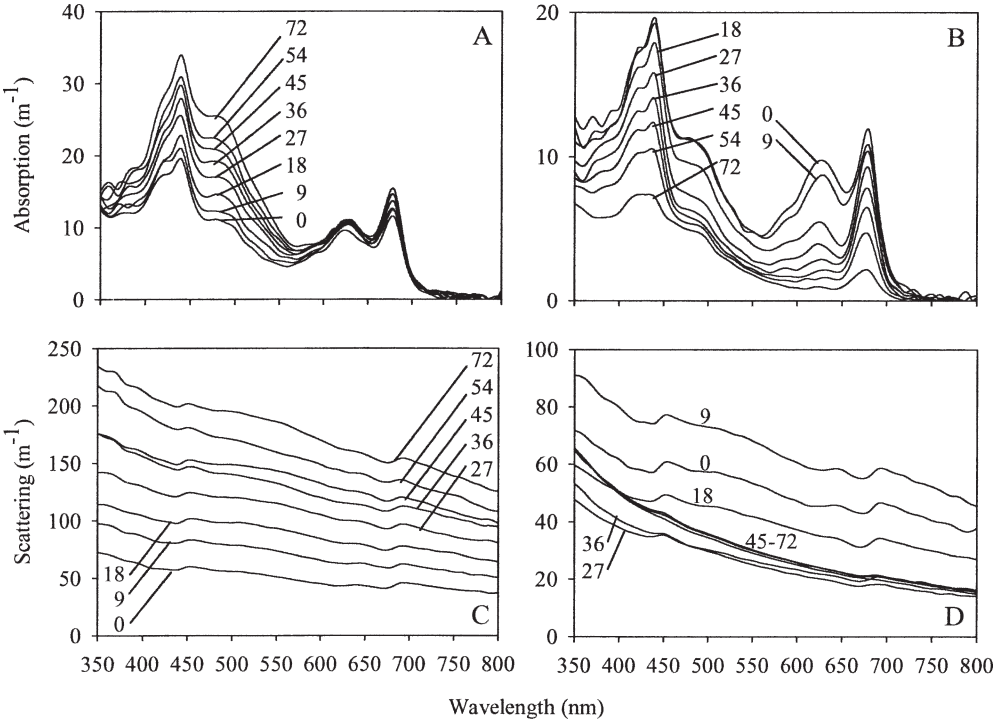

Fig. 4. (A, B) Spectra of the measured inherent optical properties absorption [$a_p(\lambda)$] and (C, D) scattering [$b_p(\lambda)$] for the infected cultures (B, D) and control culture (A, C). Sample time indicated in the plots. Spectra were smoothed over 10 nm. Note the different scales for plots of infected and control cultures.

increase in measured $b_p(\lambda)$ at $t = 9$ h, after which $b_p(\lambda)$ dropped until $t = 27$ h. Subsequently, features around the major pigment absorption peaks disappeared from the $b_p(\lambda)$ spectra. From $t = 27$ to 45 h postinfection, $b_p(\lambda)$ increased, especially toward shorter wavelengths. Between $t = 45$ and 72 h, no further changes were observed.

The number of VLP first increased sharply after 9 h postinfection (Fig. 5). Approximately 1×10^8 VLP mL^{-1} were initially added. The first measurement at $t = 0$ yielded 2×10^7 VLP mL^{-1}, indicating that most VLP rapidly attached to a host. Subsequently, VLP increased by an 18-fold measure within 18 h, coinciding with a drastic increase in the number of small particles (Fig. 3). Another outbreak of VLP occurred between 27 and 36 h postinfection. Both initial peaks in the VLP count were followed by a decline in VLP, indicating that several cycles of infection and lysis took place. At $t = 72$ h, the VLP count was 97 times higher than at $t = 0$. During the last 24-h interval (54–72 h following infection), the number of VLP increased with a factor of 7. At this point the host population was so sparse that very few new infections could occur.

The optimization of $m(\lambda)$ through ADT modeling yielded the values of $m(\lambda)$ plotted in Fig. 6. Spectral variation of the real part n was small, showing a gentle positive slope with wavelength in all samples of the control culture and the early samples of the infected cultures. These spectra were very similar to results reported by Ahn et al. (1992). Over time, the $n(\lambda)$ spectra flattened in the infected cultures. The average (±standard deviation [SD]) of $n(\lambda)$ calculated over all cultures ($n = 4$) was 1.02 ± 0.003. The imaginary part n' varied between 0 and 0.0026, with average (±SD) of 0.0007 ± 0.0005. These values of $n(\lambda)$ compare well with literature values (e.g., $n = 1.04$–1.05 for *Synechocystis* sp. and *Synechococcus* sp. [Ahn et al. 1992]; $n = 1.02$–1.04 [$\lambda = 633$] for *Microcystis* species; and $n = 1.05$ for species of the filamentous *Oscillatoria* genus [Volten et al. 1998]). In the latter study, values of n as high as 1.24 ($\lambda = 633$ nm) were found for colonies of *Prochlorothrix hollandica* (a filamentous prochlorophyte) and other colony-forming phytoplankton, supposedly because whole colonies were interpreted as single particles rather than as collections of particles. Values of $n(\lambda) > 1.15$ could also be obtained with the present data when using a PSD of volume-equivalent spheres representing whole trichomes rather than individual cells. Such high values are no longer representative of algal or bacterial particles with a relatively high water content and should be discarded as erroneous. Calculations with nonadjusted PSDs also prevented convergence of modeled and measured data in some cases, especially at shorter wavelengths. Only for the infected cultures at $t \geq 18$ h were optimized $m(\lambda)$ values approximately the same regardless of the treatment of the PSD. These infected cultures were dominated by smaller particles, including short trichomes, cell debris, and heterotrophic bacteria, so adjustment of the PSD did not have a large effect on its shape.

The calculated $b_{bp}(\lambda)$ spectra (Fig. 7) all showed a slight positive slope with wavelength, comparable to experimental and modeled results by Ahn et al. (1992). Between control (Fig. 7A,B) and infected (Fig. 7C,D) cultures, differences

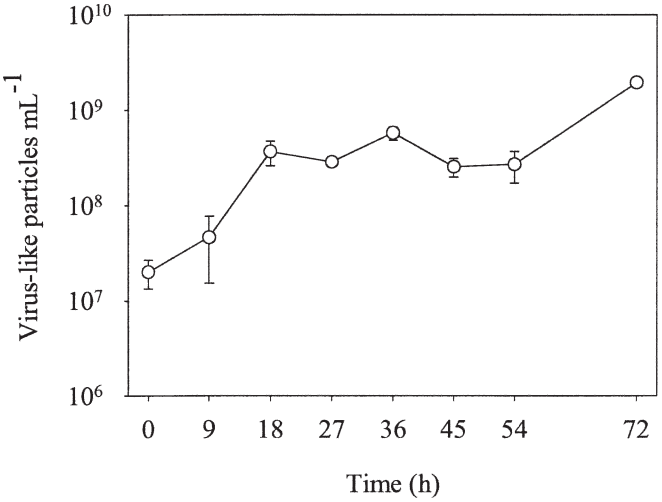

Fig. 5. Free virus-like particles (VLP) counted in the infected cultures by epifluorescence microscopy after SYBR-green staining. Error bars indicate standard deviation between replicate infected cultures ($n = 3$). The approximate number of phages added at $t = 0$ was 1.0×10^8. However, at the first count, immediately after infection ($t = 0$), the number of VLP equaled 2.0×10^7.

were largest around $t = 18$ h, marking also the first burst of free VLP and release of small cellular debris. At that time the $b_{bp}(\lambda)$ spectrum of infected cultures showed slight depressions around the blue and red absorption peaks of Chl *a*. Beyond $t = 18$ h, the backscattering intensity of these samples decreased and spectrally flattened again, simultaneous with $b_p(\lambda)$. In the control culture the $b_{bp}(\lambda)$ spectra were sloped, and spectral features around the major absorption peaks became increasingly apparent. The backscattering ratio $B(\lambda)$ was higher for infected samples (Fig. 8C,D) than for the control culture (Fig. 8A,B) from $t = 18$ h onward. Intensity and spectral shape of $B(\lambda)$ were relatively stable for the control culture.

We investigated how the calculated $b_{bp}(\lambda)$ and $B(\lambda)$ spectra were influenced by the representation of SMP in the PSD. For the infected cultures at $t = 18$ h, small particles of <0.7 μm that would not have been detected by the particle counter were added to the PSD in the model. The 'enriched' PSD and the original measurements of $a_p(\lambda)$ and $b_p(\lambda)$ were used to optimize $m(\lambda)$ for an increasing amount of SMP added to the PSD. The number of added SMP was proportional to the number of lysed *L. boryana* cells between $t = 9$ and $t = 18$ h. An enrichment factor was defined as the number of SMP added in the 0.2–0.7-μm range per lysed host cell. For enrichment factors of 0, 1, 10, 20, 30, and 50 SMP per lysed cell, Fig. 9 shows the enriched PSDs and shape factor S resulting from this approach. An enrichment factor of zero represents the original PSD after the substitution of individual particles for cells in trichomes. Because S increased in proportion to the number of added small particles, $\bar{Q}_f(\lambda)$ and $\bar{Q}_f(\lambda)$ decreased (Eq. 2), forcing a lower value for both the imaginary and the real part of the $m(\lambda)$. The increased importance of small particles, meanwhile, raised $\bar{Q}_{b_b}(\lambda)$ and, consequently

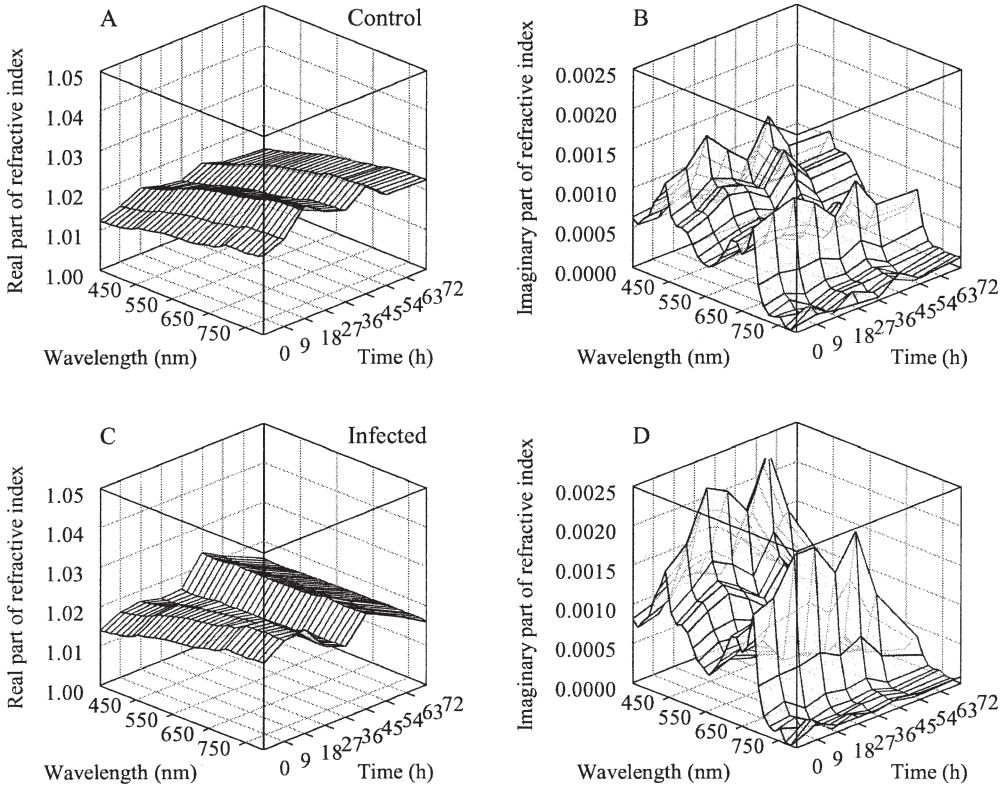

Fig. 6. (A, C) Optimized values of $m(\lambda)$, split up in real part $n(\lambda)$, and (B, C) imaginary part n' (λ) for control and infected cultures (panels A–B and C–D, respectively).

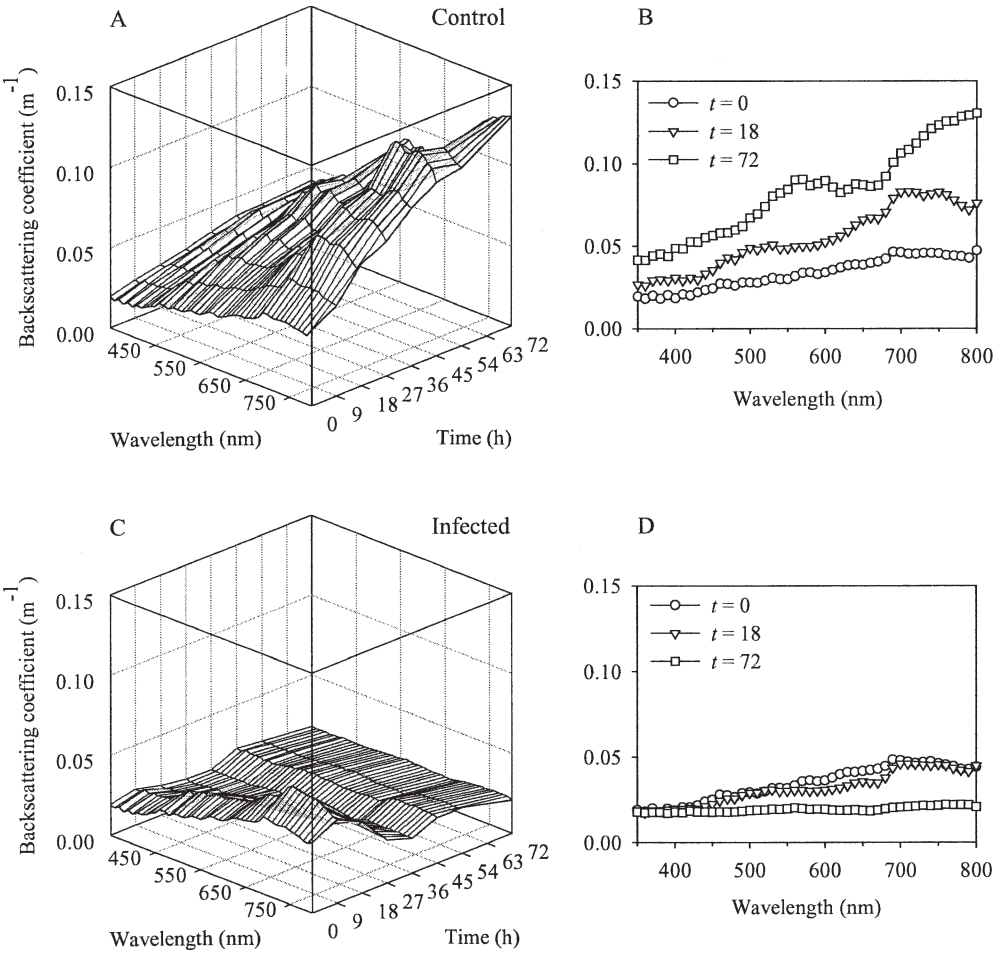

Fig. 7. (A, B) Calculated $b_{bp}(\lambda)$ spectra for uninfected and (C, D) infected cultures. Panels B and D give the spectra at t = 0, 18, and 72 h. The data is plotted at 10-nm intervals in all panels.

(through Eq. 2), $b_{bp}(\lambda)$ and $B(\lambda)$, as shown in Fig. 10. At an enrichment factor of 50, $b_{bp}(\lambda)$ and $B(\lambda)$ were approximately two times higher than with the enrichment set to zero. An enrichment factor of 50 led to a number of SMP that was one order of magnitude higher than the number of particles of ESD >0.7 μm.

In spectra of the backscattering albedo $\omega_b(\lambda)$ modeled for infected cultures (Fig. 11A), the features of absorption by PC and Chl *a* around 620 nm largely disappeared as lysis took place. At t = 18 h, $\omega_b(\lambda)$ from 700 to 800 nm reached high values, and it was particularly pronounced at 650 nm, the wavelength of the local absorption minimum between 620 nm (PC and Chl *a*) and 675 nm (Chl *a*). Until t = 36 h, $\omega_b(\lambda)$ decreased in the red and near-infrared, followed by an increase in the 550–650-nm range until the end of the experiment, while the value of $\omega_b(\lambda)$ between 750 and 800 nm dropped below the starting value. The red peak around 705 nm was very high at t = 18 and t = 54 h. In the spectral range of 350 to 500 nm, almost no change was observed throughout the experiment. In the latter region, decline of $a_p(\lambda)$ was limited, while $b_p(\lambda)$ remained relatively high, and $b_{bp}(\lambda)$ was the lowest. With increasing representation of SMP at t = 18 h, $\omega_b(\lambda)$ of the infected cultures increased and eventually doubled at an enrichment factor of 50. The virtual addition of SMP to the PSD did not change the shape of the $\omega_b(\lambda)$ spectrum [SD < 0.05 for $\omega_b(\lambda)$ spectra normalized to their maximum].

The shape of $\omega_b(\lambda)$ spectra changed markedly if $a_p(\lambda)$ and $b_{bp}(\lambda)$ were lowered relative to the absorption of water $a_w(\lambda)$. Spectra of $\omega_b(\lambda)$ are given for t = 18 h at various such 'dilutions,' for the cases excluding and including high representation (enrichment factor 50) of SMP in the PSD (Fig. 11C,D, respectively). Dilution to 10% of the original values of $a_p(\lambda)$ and $b_{bp}(\lambda)$ yielded spectra that are representative of well-mixed eutrophic lakes, whereas the undiluted spectra (indicated with 100%) are comparable with hypertrophic systems with surfacing blooms (cf. Rijkeboer et al. 1998). It is noted that effects of optically active substances that were not present in our cultures, such as suspended minerals, most organic detritus, CDOM, and also of bottom reflectance on $\omega_b(\lambda)$, were not considered. As a result of the strong absorption by water, diluting the culture suspensions would primarily cause lower $\omega_b(\lambda)$ at wavelengths >700 nm. Dilutions from 50% to 10% also lowered $\omega_b(\lambda)$ between 550 and 675 nm. Only at the strongest dilution considered (1%) was a decrease of $\omega_b(\lambda)$ down to 450 nm noticed. With increasing dilution,

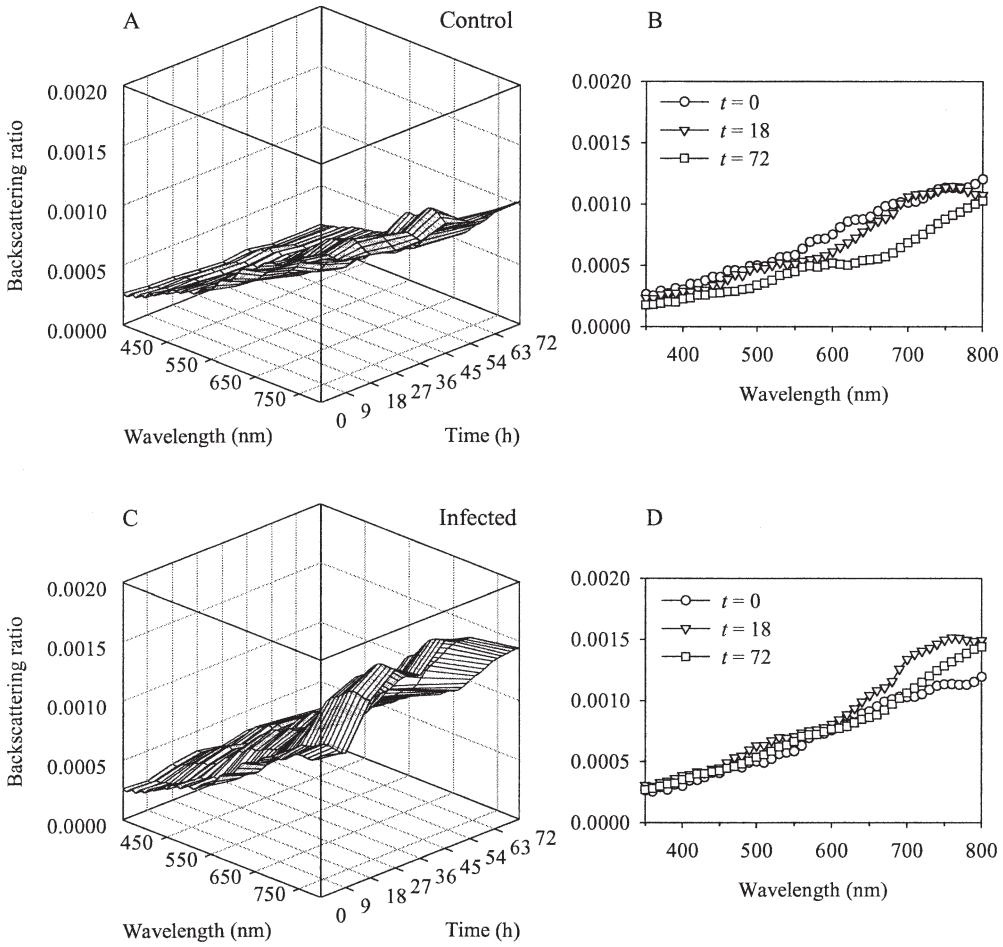

Fig. 8. Backscattering ratios $B(\lambda)$ derived from measured $b_p(\lambda)$ (Fig. 4C,D) and modeled $b_{bp}(\lambda)$ (Fig. 7) for (A, B) uninfected and (C, D) infected cultures. Panels B and D give the spectra at t = 0, 18, and 72 h. The data is plotted at 10-nm intervals in all panels.

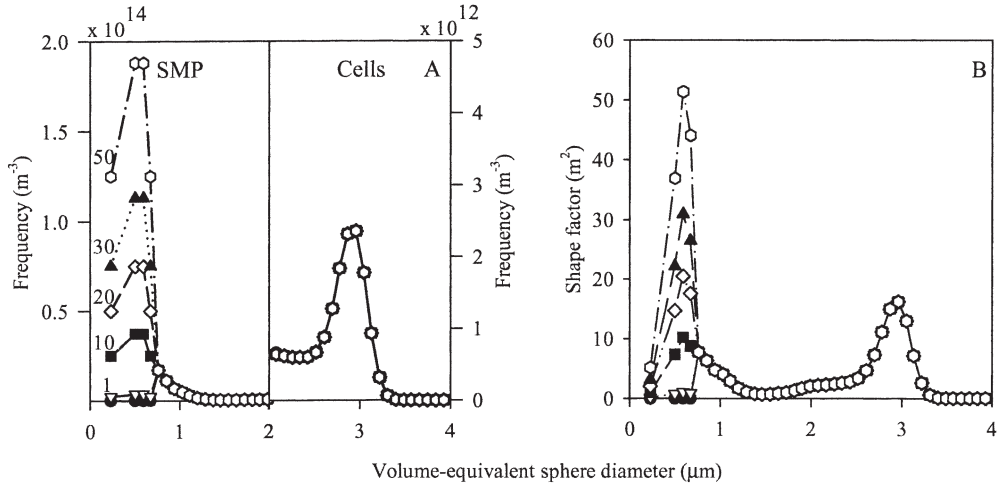

Fig. 9. PSDs used to test the effect of increasing representation of SMP (<0.7 μm) in the PSD on the amplitude of $b_{bp}(\lambda)$ for the infected cultures at t = 18 h. (A) PSD for the case of 0 (no change), 1, 10, 20, 30, and 50 small particles for every cell that was lysed in the 9–18-h interval. (B) Geometric shape S of the PSDs in panel A (Eq. 1).

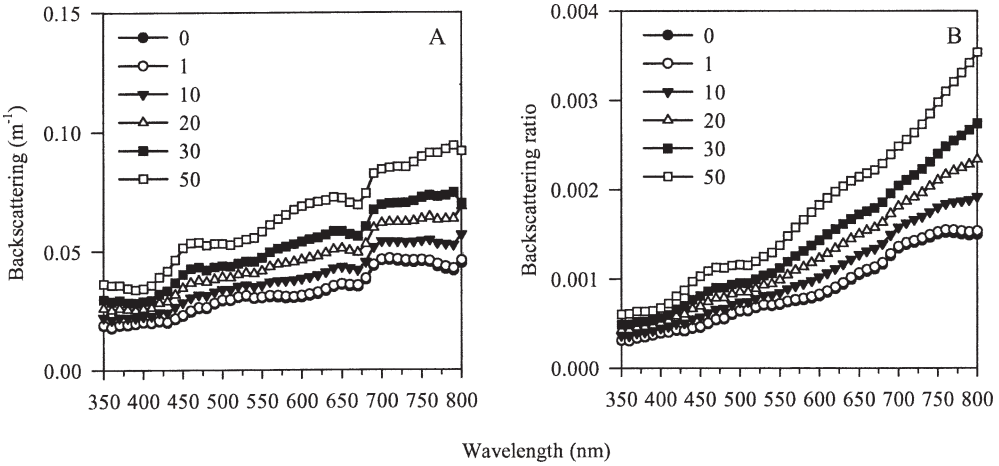

Fig. 10. Modeled spectra of (A) $b_{bp}(\lambda)$ and (B) $B(\lambda)$ as a function of SMP representation in the PSD for $t = 18$ h (Fig 9). The data is plotted at 10-nm intervals.

the peaks in the $\omega_b(\lambda)$ spectra shifted to shorter wavelengths. At 10% dilutions, changes in $\omega_b(\lambda)$ following infection of the cultures were insignificant below 450 nm and above 750 nm (Fig. 11E), but the green peak around 550 nm became more pronounced. At the 10% dilution it is easy to follow the dynamics of waveband ratios that are used for remote sensing of the photosynthetic pigments Chl *a* and PC. The ratio of reflectance bands recorded by the Medium Resolution Imaging Spectrometer (MERIS) on the ENVISAT satellite is 709 : 665 nm to detect Chl *a* (Gons et al. 2005). The retrieval of PC can be based on the ratio of bands 709 : 620 nm (Simis et al. 2005*a*). It was observed (Fig. 11F) that the band ratio indicative for PC declined more rapidly than the band ratio for Chl *a* retrieval, which is in accordance with previously published results on the PC : Chl *a* pigment ratio during lysis of cyanobacteria in enclosed lake water (Simis et al. 2005*b*).

Discussion

Previous studies have pointed out that live cells of most phytoplankton species, and cyanobacteria in particular, have a weak influence on the backscattered light signal, whereas detritus particles and bacteria may contribute most to particulate backscattering (Morel and Ahn 1991; Stramski and Kiefer 1991; Ahn et al. 1992; Stramski and Mobley 1997). During a cyanobacterial bloom, mass viral lysis can dramatically alter the nature of the dominant scattering particles, and backscattering may become more important as a result of a shift of the particle size distribution toward smaller particles, including heterotrophic bacteria degrading the lytic material. It was shown in this work that under the assumption of homogeneous spheres representing cells organized in cyanobacterial trichomes, the backscattering ratio remained low throughout an experimental mass lysis event. A more significant increase of the backscattering ratio was found when the presence of a very large release of submicron cell debris, not visible to the particle sizer but possibly present, was accounted for. In all cases, however, the increased importance of small particulate matter did not markedly alter the spectral shape of modeled backscattering. The optimized values of the refractive index remained low throughout lysis, with or without enrichment of the PSD with small particles, which indicates that the dominant particles were indeed weak scatterers. It was previously shown that $m(\lambda)$ is largely dependent on cell material and relative water content (Aas 1996). The cellular structure and biochemical composition of *L. boryana* is not expected to be essentially different from previously studied cyanobacterial species, and indeed the optimized values of $m(\lambda)$ compared reasonably well with expectations raised from earlier reports (Ahn et al. 1992; Volten et al. 1998).

Absence of strong absorption in the CDOM fraction as a result of lysis was likely the result of the presence of heterotrophic bacteria. They existed in the cultures to prevent released water-soluble phycobilin pigments from discoloring the medium, in order to retain relevance to earlier findings with enclosed lake water (Simis et al. 2005*b*). A positive response of the heterotrophic bacterial community exists upon lysis of the dominant cyanobacterial host in such enclosures (Van Hannen et al. 1999; Tijdens et al. unpubl. data). In the cultures of *L. boryana*, heterotrophic bacteria normally grow at low densities on exudates and cellular debris. The influence of the bacteria on the bulk optical properties could be significant toward the end of the lysis experiment as lysis induced an increase in their numbers, but these observations lack sufficient detail to be certain. It is likely that the release of lytic products was at least in part countered by heterotrophic bacterial activity, as can also be expected during lysis of natural blooms. In nature the rate of degradation will depend largely on the food quality of the released organic matter for the heterotrophic bacterial community and higher trophic levels.

Changes in the color (hue and brightness) of a water body can be recorded using current remote sensors placed on ships, aircraft, or satellites. Bio-optical models relate the contribution of the various water constituents to the spectral reflectance of a water body. The optical behavior of phytoplankton blooms is still insufficiently known to correctly interpret remotely sensed signals in terms of

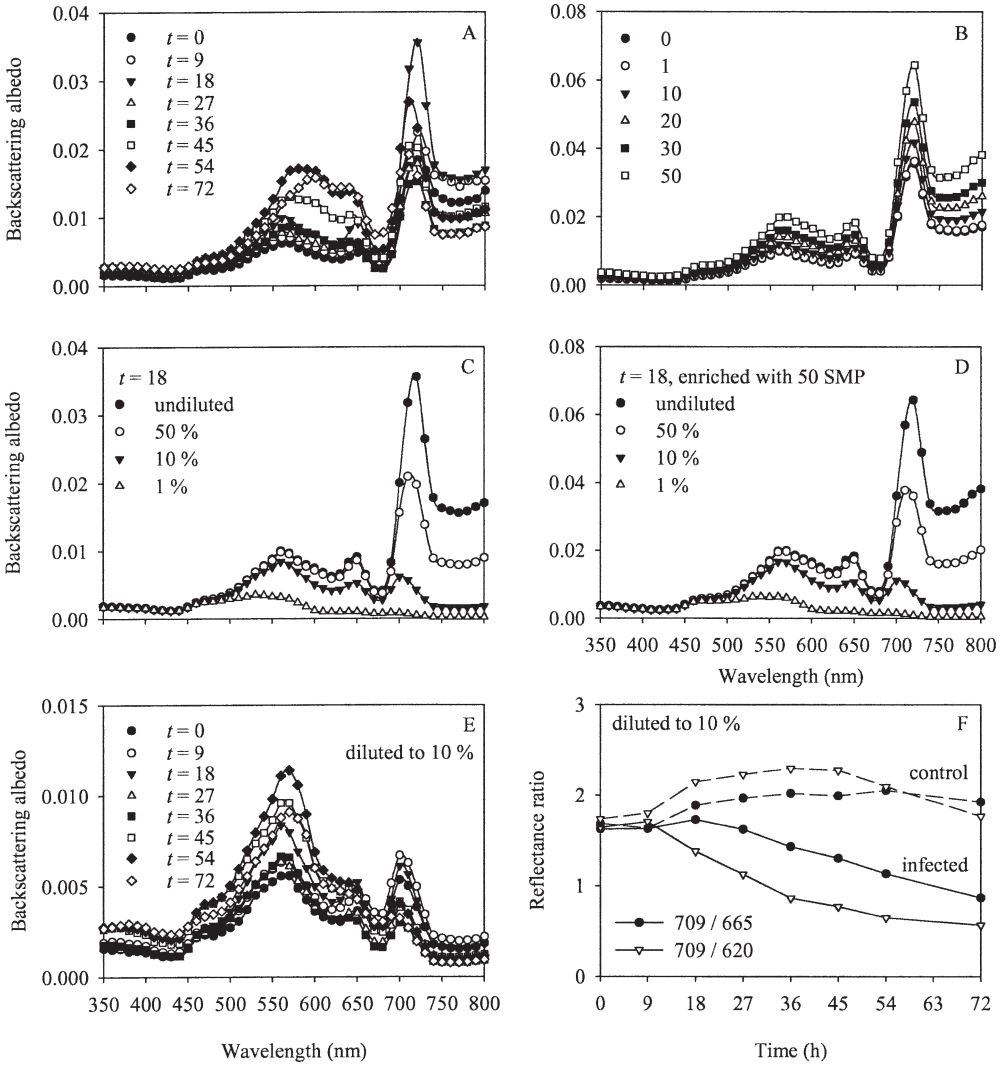

Fig. 11. Modeled reflectance $\omega_b(\lambda)$ (*see Methods*) for infected cultures using (A) $b_{bp}(\lambda)$ from Fig. 7C and (B) $b_{bp}(\lambda)$ from Fig. 10A (t = 18 h, varying representation of SMP in the PSD). Reflectances of panel A at t = 18 h and panel B at enrichment factor 50 are shown in C and D for various dilutions (as indicated) of the optical properties $a_p(\lambda)$ and $b_{bp}(\lambda)$ relative to the absorption by pure water $a_w(\lambda)$. (E) Dilutions to 10% of the time series displayed in panel A. (F) Ratios of bands 709 : 665 nm and 709 : 620 nm, used for, respectively, chlorophyll *a* and phycocyanin retrieval from remotely sensed imagery, based on the 10% dilution series (panel E).

bloom dynamics. It was previously found that drastic changes in the inherent optical properties $a_p(\lambda)$ and $b_p(\lambda)$ occurred upon mass lytic activity in nutrient-induced blooms of a filamentous cyanobacterial community (Gons et al. 2002; Simis et al. 2005*b*). As a result of the magnitude of these changes, it was postulated that they could be identified using satellite-borne remote sensors. To date, it is not known whether these lytic events can be distinguished from other mortality factors based on water color data, although the rate at which viral lysis is able to reduce a host population is unparalleled.

Measures for spectral reflectance of a water body can be predicted from the inherent optical properties $a_p(\lambda)$ and $b_{bp}(\lambda)$. The backscattering albedo $\omega_b(\lambda)$ was obtained by combining modeled and measured results and allows evaluation of the spectral changes in the upwelling light during the lysis experiment. Because of low values of the refractive index and the absence of marked spectral changes of $b_{bp}(\lambda)$ as a result of lysis, changes in $\omega_b(\lambda)$ were dominated by changes in the absorption of the water constituents and by the importance of their absorption relative to water. The intensity of the $\omega_b(\lambda)$ spectra did show a positive linear response to inclusion of SMP in the PSD (i.e., particles that could have been present below the detection limit of the particle sizer). The spectral shape of $b_{bp}(\lambda)$ was not markedly affected by the inclusion of SMP in these experiments, however, and $\omega_b(\lambda)$ was only significantly elevated when very high population densities were considered, or when many SMP were included. Still, the amount of released SMP as well as the rate of degradation of this material and, thus, the time of observation can have a significant effect on the amplitude of the reflected light

signal. The intensity of reflectance is therefore not considered a consistent indicator of mass lysis events.

Spectral changes in $\omega_b(\lambda)$ revealed a more pronounced 'green peak' of reflectance at λ = 560 to 600 nm, as was also observed earlier with enclosed lake water using a generic VSF (Petzold 1977) to calculate reflectance spectra (Simis et al. 2005*b*). This spectral change is explained jointly by relatively small changes of $a_p(\lambda)$ and $b_p(\lambda)$ in the blue spectral domain, an increase in $b_{bp}(\lambda)$ toward longer wavelengths, and the disappearance of absorption by photosynthetic pigments in the red spectral domain. The typical absorption features of PC and Chl *a* underwent significant changes that may be retrieved by reflectance band ratios recorded over turbid water bodies (Gons et al. 2005; Simis et al. 2005*a*). The band ratios 709 : 665 nm for Chl *a* and 709 : 620 nm for PC retrieval dropped as pigments were released and small particles degraded. The band ratio indicating PC absorption dropped more rapidly than the band ratio for Chl *a,* as explained above. This observation is in agreement with measurements of the concentrations of these pigments in lysis studies of enclosed lake water (Gons et al. 2002; Simis et al. 2005*b*). The sudden release of small cell debris may be marked as a main difference between viral mortality and other mortality causes (zooplankton grazing, cell senescence, fungal infection), but it had only a brief effect on the amplitude of the reflectance spectra. It thus appears that regardless of the dynamics in the amplitude of the reflected light signal that cause the $\omega_b(\lambda)$ spectra to shift up and down in a less predictable manner, the ratio of PC to Chl *a* is most useful to follow mass lysis of cyanobacteria in time. When the pigment balance drops rapidly (i.e., within days), mass viral lysis is the most likely mortality factor.

In conclusion, the present work contains the first optical modeling of the scattering behavior during mass viral lysis of phototrophs. It was possible to show temporal trends in the modeled backscattering behavior of a population of cyanobacteria undergoing mass viral lysis. Although the use of the Mie scattering model is widespread in hydrological modeling, giving insight in the scattering behavior of polydisperse populations of nonspherical particles, the modeled results at backward scattering angles should always be treated with scrutiny (Stramski et al. 2004, and references therein). Scattering models for irregularly shaped particles exist (Mishchenko et al. 2002), but the added complexity brings higher computational needs, and no scattering model can be expected to precisely describe the optical behavior of complex biological particles. For example, the internal structure of cyanobacterial cells is relatively simple compared to eukaryotic phytoplankton, but inhomogeneous distribution of the absorbing photosynthetic pigments may be observed in filamentous species like *L. boryana*. Fluorescence has also not been taken into account in these scattering models but can be a significant component of the upwelling light in clear water systems as well as in measurements of $b_{bp}(\lambda)$ of cultured species (Ahn et al. 1992). Above all, it is encouraged that (1) optical modeling of mass lysis of phytoplankton is carried out for other cultured species, and (2) such studies are validated with actual measurements of the VSF, preferably at several key wavelengths. Despite these considerations, it is believed that the optical characteristics of lysis of a phytoplankton bloom, a situations where the light field is dominated first by a dense host and then by lytic products, bacteria, and viruses, may be approximated by applying these simplifying scattering models, especially where temporal trends in the scattering data are considered.

The present results can be implemented in bio-optical models that also incorporate other optically active water constituents: plankton species unaffected by the ongoing viral lysis, CDOM, and suspended sediments. Remote sensing studies may thus focus on bloom dynamics both as blooms first appear on imagery and as they fade or disappear. This information may lead to better understanding of the conditions under which mass lytic events occur. Hypoxia following release of organic matter, and the possible release of harmful substances produced by algal and cyanobacterial species, warrant special attention with regard to the causes of mass viral lysis and general bloom dynamics.

References

Aas, E. 1996. Refractive index of phytoplankton derived from its metabolite composition. J. Plankton Res. **18:** 2223–2249.

Ahn, Y. H., A. Bricaud, and A. Morel. 1992. Light backscattering efficiency and related properties of some phytoplankters. Deep-Sea Res. **39:** 1835–1855.

Anagnostidis, K., and J. Komárek. 1988. Modern approach to the classification system of cyanophytes.3—Oscillatoriales. Arch. Hydrobiol. (suppl.) **80:** 327–472.

Babin, M., and D. Stramski. 2002. Light absorption by aquatic particles in the near-infrared spectral region. Limnol. Oceanogr. **47:** 911–915.

———, and ———. 2004. Variations in the mass-specific absorption coefficient of mineral particles suspended in water. Limnol. Oceanogr. **49:** 756–767.

Balch, W. M., and others. 2002. Fundamental changes in light scattering associated with infection of marine bacteria by bacteriophage. Limnol. Oceanogr. **47:** 1554–1561.

Bergh, Ø., K. Y. Børsheim, G. Bratbak, and M. Heldal. 1989. High abundance of viruses found in aquatic environments. Nature **340:** 467–468.

Bohren, C. F., and D. R. Huffman. 1983. Absorption and scattering of light by small particles. Wiley.

Bricaud, A., A. L. Bedhomme, and A. Morel. 1988. Optical properties of diverse phytoplanktonic species—experimental results and theoretical interpretation. J Plankton Res. **10:** 851–873.

———, A. Morel, and L. Prieur. 1983. Optical efficiency factors of some phytoplankters. Limnol. Oceanogr. **28:** 816–832.

Brussaard, C. P. D. 2004. Viral control of phytoplankton populations—a review. J. Eukaryot. Microbiol. **51:** 125–138.

Buiteveld, H., J. H. M. Hakvoort, and M. Donze. 1994. The optical properties of pure water. SPIE Proc. Ocean Optics XII **2258:** 174–183.

Gons, H. J., J. Ebert, H. L. Hoogveld, L. Van den Hove, R. Pel, W. Takkenberg, and C. J. Woldringh. 2002. Observations on cyanobacterial population collapse in eutrophic lake water. Antonie Leeuwenhoek Int. J. G. **81:** 319–326.

———, M. Rijkeboer, and K. G. Ruddick. 2005. Effect of a waveband shift on chlorophyll retrieval from MERIS imagery of inland and coastal waters. J. Plankton Res. **27:** 125–127.

Gordon, H. R., O. B. Brown, and M. M. Jacobs. 1975. Computed relationships between the inherent and apparent optical properties of a flat homogeneous ocean. Appl. Optics **14:** 417–427.

Latimer, P., A. Brunsting, B. E. Pyle, and C. Moore. 1978. Effects of asphericity on single particle scattering. Appl. Optics **17:** 3152–3158.

Maske, H., and H. Haardt. 1987. Quantitative in vivo absorption spectra of phytoplankton: Detrital absorption and comparison with fluorescence excitation spectra. Limnol. Oceanogr. **32:** 620–633.

Mie, G. 1908. Contribution on optical properties of turbid solutions, with special reference to colloidal metallic solutions. Ann. Phys. **25:** 337–445.

Mishchenko, M. I., L. D. Travis, and A. A. Lacis. 2002. Scattering, absorption, and emission of light by small particles. Cambridge Univ. Press.

Morel, A., and Y.-H. Ahn. 1991. Optics of heterotrophic nanoflagellates and ciliates: A tentative assessment of their scattering role in oceanic waters compared to those of bacteria and algal cells. J. Mar. Res. **49:** 177–202.

———, and A. Bricaud. 1986. Inherent properties of algal cells including picoplankton: Theoretical and experimental results, p. 521–559. *In* T. Platt and W. K. W. Li [eds.], Photosynthetic picoplankton. Can. Bull. Fish. Aquat. Sci. **214.**

———, and B. Gentili. 1991. Diffuse reflectance of oceanic waters—its dependence on sun angle as influenced by the molecular-scattering contribution. Appl. Optics **30:** 4427–4438.

———, and ———. 1993. Diffuse-reflectance of oceanic waters.2. Bidirectional aspects. Appl. Optics **32:** 6864–6879.

Noble, R. T., and J. A. Fuhrman. 1998. Use of SYBR Green I for rapid epifluorescence counts of marine viruses and bacteria. Aquat. Microb. Ecol. **14:** 113–118.

Petzold, T. 1977. Volume scattering functions for selected ocean waters, p. 152–174. *In* J. E. Tyler [ed.], Light in the sea. Dowden, Hitchinsons and Ross.

Proctor, L. M., and J. A. Fuhrman. 1990. Viral mortality of marine-bacteria and cyanobacteria. Nature **343:** 60–62.

Rijkeboer, M., A. G. Dekker, and H. J. Gons. 1998. Subsurface irradiance reflectance spectra of inland waters differing in morphometry and hydrology. Aquat. Ecol. **31:** 313–323.

Safferman, R. S., and M. E. Morris. 1964. Growth characteristics of the blue-green algal virus LPP-1. J. Bacteriol. **88:** 771–775.

Segelstein, D. J. 1981. The complex refractive index of water. M.Sc. thesis, Univ. of Missouri-Kansas City.

Shibata, A., K. Kogure, I. Koike, and K. Ohwada. 1997. Formation of submicron colloidal particles from marine bacteria by viral infection. Mar. Ecol. Prog. Ser. **155:** 303–307.

Simis, S. G. H., S. W. M. Peters, and H. J. Gons. 2005*a*. Remote sensing of the cyanobacterial pigment phycocyanin in turbid inland water. Limnol. Oceanogr. **50:** 237–245.

———, M. Tijdens, H. L. Hoogveld, and H. J. Gons. 2005*b*. Optical changes associated with cyanobacterial bloom termination by viral lysis. J. Plankton Res. **27:** 937–949.

Stramski, D., E. Boss, D. Bogucki, and K. J. Voss. 2004. The role of seawater constituents in light backscattering in the ocean. Prog. Oceanogr. **61:** 27–56.

———, and D. A. Kiefer. 1991. Light-scattering by microorganisms in the open ocean. Prog. Oceanogr. **28:** 343–383.

———, and C. D. Mobley. 1997. Effects of microbial particles on oceanic optics: A database of single-particle optical properties. Limnol. Oceanogr. **42:** 538–549.

———, A. Morel, and A. Bricaud. 1988. Modeling the light attenuation and scattering by spherical phytoplanktonic cells—a retrieval of the bulk refractive-index. Appl. Optics **27:** 3954–3956.

———, and R. A. Reynolds. 1993. Diel variations in the optical-properties of a marine diatom. Limnol. Oceanogr. **38:** 1347–1364.

———, and S. B. Wozniak. 2005. On the role of colloidal particles in light scattering in the ocean. Limnol. Oceanogr. **50:** 1581–1591.

Suttle, C. A. 1994. The significance of viruses to mortality in aquatic microbial communities. Microb. Ecol. **28:** 237–243.

Ulloa, O., S. Sathyendranath, and T. Platt. 1994. Effect of the particle-size distribution on the backscattering ratio in seawater. Appl. Optics **33:** 7070–7077.

Van Hannen, E. J., G. Zwart, M. P. Van Agterveld, H. J. Gons, J. Ebert, and H. J. Laanbroek. 1999. Changes in bacterial and eukaryotic community structure after mass lysis of filamentous cyanobacteria associated with viruses. Appl. Environ. Microbiol. **65:** 795–801.

Van de Hulst, H. C. 1957. Scattering of light by small particles. Wiley.

Volten, H., and others. 1998. Laboratory measurements of angular distributions of light scattered by phytoplankton and silt. Limnol. Oceanogr. **43:** 1180–1197.

Wilson, W. H., N. G. Carr, and N. H. Mann. 1996. The effect of phosphate status on the kinetics of cyanophage infection in the oceanic cyanobacterium *Synechococcus* sp WH7803. J. Phycol. **32:** 506–516.

———, and N. H. Mann. 1997. Lysogenic and lytic viral production in marine microbial communities. Aquat. Microb. Ecol. **13:** 95–100.

———, S. Turner, and N. H. Mann. 1998. Population dynamics of phytoplankton and viruses in a phosphate-limited mesocosm and their effect on DMSP and DMS production. Estuar. Coast. Shelf Sci. **46:** 49–59.

Received: 23 January 2006
Accepted: 12 September 2006
Amended: 12 September 2006